MAPPING THE FRINGE FIELDS OF MULTIPOLE MAGNETS*

E. A. Wadlinger

MS-H808, Los Alamos National Laboratory, Los Alamos, NM 87545

Abstract

A good method for mapping multipole magnets (suggested by K. Halbach) is to measure the magnetic field on the surface of a constant radius cylinder centered on the magnet axis. This paper presents one approach to this mapping concept using a magnetic field description that identically satisfies Maxwell's equations. The field map is used to determine the magnetic scalar potential function written in a form that reduces to a standard multipole expansion for an axially independent field. This scalar potential function is used in particle tracking codes. An example and a brief error analysis are included.

Mapping Method

Figure 1 illustrates the mapping method using sensing coils (Hall probe mapping is conceptually the same as the coil method). Coils C_r and C_θ, which measure changes in the radial and azimuthal magnetic flux through the coils during angular coil rotation, are stepped axially through the magnet including the fringe-field region. At each axial position, the cylinder holding the sensing coils is rotated and the changes in magnetic flux versus angle are measured and Fourier analyzed. The Fourier amplitudes are used to determine the magnetic scalar potential function (see below). The axial length δz_C of the sensing coils should be small compared to the magnet aperture in order to measure the magnet fringe field with maximum experimental sensitivity and to simplify the analysis.
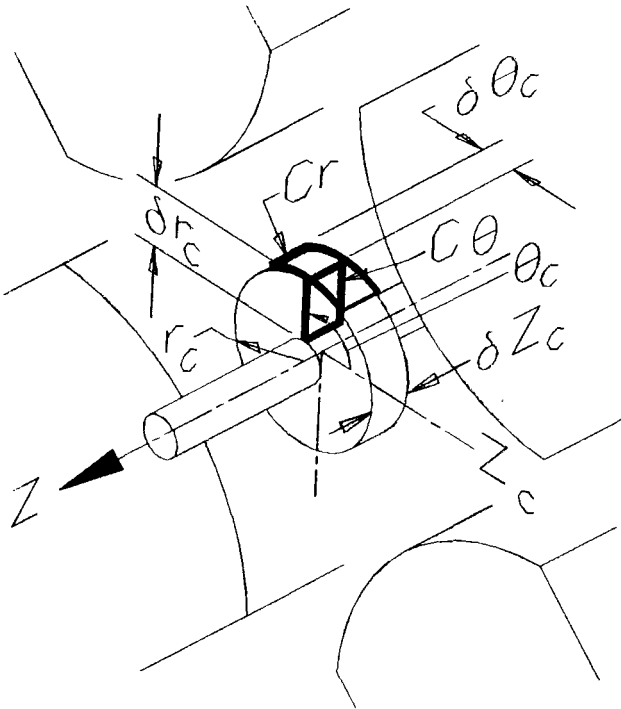
Fig. 1. Schematic of magnet-mapping coil geometry.

Signals from C_r and C_θ are proportional to the change in the total magnetic flux ($\partial\Phi/\partial\theta$) through the coils during rotation. The magnetic flux measurements, at axial coil position $z_C = z_i$ ($i = 1,...,$ number of measurements), are Fourier analyzed to give the amplitudes A and B at each location where

$$\frac{\partial\Phi_{C_r}}{\partial\theta_C}\Big|_{z_C=z_i} = \sum_m \left[A_{r_m}(z_i)\sin(m\theta_C) + B_{r_m}(z_i)\cos(m\theta_C) \right] , \quad (1)$$

$$\frac{\partial\Phi_{C_\theta}}{\partial\theta_C}\Big|_{z_C=z_i} = \sum_m \left[A_{\theta_m}(z_i)\sin(m\theta_C) + B_{\theta_m}(z_i)\cos(m\theta_C) \right] , \quad (2)$$

(m is an integer denoting the harmonic number; subscript r refers to the radial flux measurement; subscript θ refers to the azimuthal measurement; and θ_C is the coil angle). If the coils contain multiple loops, the measured values must be divided by the number of loops.

Analysis Equations

The magnetic field in a source-free region can be calculated from a scalar (V) potential function where, in cylindrical coordinates,

$$\vec{B} = -\nabla V = -\left(\hat{a}_r \partial_r + \hat{a}_\theta \frac{\partial_\theta}{r} + \hat{k}\partial_z \right) V \quad (3)$$

(∂_r denotes the partial derivative with respect to r, etc., and the $\hat{a}$'s are unit vectors in cylindrical coordinates). Because $\nabla\cdot\vec{B} = 0$ in a source-free region, the scalar potential satisfies the Laplace equation and can be written as[1]

$$V(r,\theta,z) = \sum_m \left(\frac{r}{r_a}\right)^m \sum_{n=0}^\infty \frac{m!(-r^2\partial_z^2)^n}{2^{2n}n!(n+m)!}$$
$$\times \; [\cos(m\theta)F_m(z) + \sin(m\theta)G_m(z)] \quad , \quad (4)$$

where r_a is the magnet aperture radius. The scalar potential in Eq. (4), which consists of a power series expansion in r for each harmonic number m, is fully determined by the arbitrary nonsingular functions $F_m(z)$ and $G_m(z)$. These nonsingular functions satisfy the boundary conditions that all the derivatives of F and G vanish at $z \to \pm\infty$. (Periodic boundary conditions can also be imposed as in the example given later.) In SI units, V has the dimensions of tesla-meters; therefore, F_m and G_m also have the units of tesla-meters. [Note that $(r^2\partial_z^2)$ is dimensionless.]

Equations (3) and (4) are combined to obtain the magnetic field. We ignore B_z and concentrate on B_r and B_θ. The total flux Φ through the coils C_r and C_θ, determined from the area integrals, is

$$\Phi_{C_r} = \int_{\theta_C-\delta\theta_C}^{\theta_C+\delta\theta_C} r_C d\theta \int_{z_C}^{z_C+\delta z_C} B_r dz|_{r=r_C} ; \quad (5)$$

$$\Phi_{C_\theta} = \int_{r_C-\delta r_C}^{r_C} dr \int_{z_C}^{z_C+\delta z_C} B_\theta dz|_{\theta=\theta_C} . \quad (6)$$

Measurements of $\partial\Phi/\partial\theta$ are made at various z positions (the highest density of measurements are made in the magnet fringe-field region where F and G are rapidly varying). From Eqs. (5) to (6) and rearranging, we have

$$\frac{\partial \Phi_{C_r}}{\partial \theta_C} = \sum_m \sum_{n=0}^{\infty} K_r(m,n) \int_{z_C}^{z_C + \delta z_C}$$

$$\left[\sin(m\theta_C)r_C^{2n}\partial_z^{2n}F_m(z) - \cos(m\theta_C)r_C^{2n}\partial_z^{2n}G_m(z)\right]dz , \quad (7)$$

$$\frac{\partial \Phi_{C_\theta}}{\partial \theta_C} = \sum_m \sum_{n=0}^{\infty} K_\theta(m,n) \int_{z_C}^{z_C + \delta z_C}$$

$$\left[\cos(m\theta_C)r_C^{2n}\partial_z^{2n}F_m(z) + \sin(m\theta_C)r_C^{2n}\partial_z^{2n}G_m(z)\right]dz , \quad (8)$$

where

$$K_r(m,n) = \frac{\sin(m\delta\theta_C)(-1)^n(m+2n)m!}{2^{2n-1}n!(n+m)!}\frac{r_C^m}{r_a^m}, \quad (9)$$

$$K_\theta(m,n) = \frac{(-1)^n m^2 m!\left[1 - \left(\frac{r_C - \delta r_C}{r_C}\right)^{m+2n}\right]}{2^{2n}(m+2n)n!(n+m)!}\frac{r_C^m}{r_a^m} \quad (10)$$

are independent of z and dimensionless. (The z partial derivatives can be written as total derivatives inside the above integrals. The partial derivative symbol is retained to enhance readability.)

We use a Taylor series expansion

$$F(z_0 + \delta z_C) = \sum_{j=0}^{\infty} \frac{1}{j!}[\partial_z^j F(z)]_{z=z_0}(\delta z_C)^j \quad (11)$$

to determine the integrals in Eqs. (7) and (8). Using the notation $F_m^{(n)}(z) = \partial_z^n F_m(z)$, then

$$\int_{z_C}^{z_C + \delta z_C} \partial_z^{2n} F_m(z)dz = \sum_{j=1}^{\infty} \frac{F_m^{(2n+j-1)}(z_C)(\delta z_C)^j}{j!}$$

$$= F_m^{(2n)}(z_C)\delta z_C + ... \quad (12)$$

Substitute Eq. (12) into Eqs. (7) and (8), then compare with Eqs. (1) and (2) to define

$$A_{r_m}^a(z_C) = +\sum_{n=0}^{\infty} K_r(m,n)r_C^{2n}\sum_{j=1}^{\infty}\frac{\partial_{z_C}^{2n+j-1}F_m(z_C)(\delta z_C)^j}{j!} , \quad (13)$$

$$B_{r_m}^a(z_C) = -\sum_{n=0}^{\infty} K_r(m,n)r_C^{2n}\sum_{j=1}^{\infty}\frac{\partial_{z_C}^{2n+j-1}G_m(z_C)(\delta z_C)^j}{j!} , \quad (14)$$

$$A_{\theta_m}^a(z_C) = +\sum_{n=0}^{\infty} K_\theta(m,n)r_C^{2n}\sum_{j=1}^{\infty}\frac{\partial_{z_C}^{2n+j-1}G_m(z_C)(\delta z_C)^j}{j!} , \quad (15)$$

$$B_{\theta_m}^a(z_C) = +\sum_{n=0}^{\infty} K_\theta(m,n)r_C^{2n}\sum_{j=1}^{\infty}\frac{\partial_{z_C}^{2n+j-1}F_m(z_C)(\delta z_C)^j}{j!} , \quad (16)$$

which have the dimensions of Webers (tesla-meters^2). The superscripts a indicate that the A^a and B^a terms refer to the analytic expressions, Eqs. (13) to (16). These A and B terms should agree with those in Eqs. (1) and (2) to within the experimental measurement accuracy. The measured A and B coefficients in Eqs. (1) and (2) are used to determine the F and G functions in Eqs. (13) to (16) (see below).

Equations (13) to (16) contain the full power series expansion in terms of the pickup loop width δz_C. Usually, only the first order term in δz_C of the power series expansion is required.

Tables I and II are given to provide some indication as to how rapidly the power series, in n, in Eqs. (7), (8), and (13) to (16) converge. We assume, in these tables, that $r_C = \delta r_C = r_a$ and $\sin(m\delta\theta_C) = 1$. (The series will converge more rapidly for

TABLE I. FUNCTION $K_r(m,n)$.

m	n						
	0	1	2	3	4	5	6
1	2.0E+00	-7.5E-01	5.2E-02	-1.5E-03	2.4E-05	-2.5E-07	1.7E-09
2	4.0E+00	-6.7E-01	3.1E-02	-6.9E-04	9.0E-06	-7.8E-08	4.7E-10
3	6.0E+00	-6.3E-01	2.2E-02	-3.9E-04	4.3E-06	-3.1E-08	1.7E-10
4	8.0E+00	-6.0E-01	1.7E-02	-2.5E-04	2.3E-06	-1.5E-08	7.2E-11
5	1.0E+01	-5.8E-01	1.3E-02	-1.7E-04	1.4E-06	-8.1E-09	3.5E-11

TABLE II. FUNCTION $K_\theta(m,n)$.

m	n						
	0	1	2	3	4	5	6
1	1.0E+00	-4.2E-02	1.0E-03	-1.6E-05	1.5E-07	-1.0E-09	5.2E-12
2	2.0E+00	-8.3E-02	1.7E-03	-2.2E-05	1.8E-07	-1.1E-09	4.8E-12
3	3.0E+00	-1.1E-01	2.0E-03	-2.2E-05	1.6E-07	-8.4E-10	3.4E-12
4	4.0E+00	-1.3E-01	2.1E-03	-2.0E-05	1.3E-07	-6.2E-10	2.2E-12
5	5.0E+00	-1.5E-01	2.1E-03	-1.8E-05	1.0E-07	-4.5E-10	1.5E-12

$r_C < r_a$.) Table I tabulates $K_r(m,n)$ and Table II tabulates $K_\theta(m,n)$.

Functions F and G are generally smooth and well behaved with derivatives that rapidly become small with increasing order. Tables I and II indicate that the power series expansions (in n) in Eqs. (13) to (16) can be terminated at low values for n.

Fitting Procedure

We use the magnetic field measurements, in the form of Eqs. (1) and (2), and Eqs. (13) to (16) to determine the F_m and G_m functions; F_m and G_m can be any function of z that is nonsingular and satisfies the appropriate boundary conditions. (In some cases, analytic expressions exist[1,2] for F and G.) A series expansion using "model" functions can be made for F and G. Then, Eqs. (13) to (16) together with the magnet map will determine the expansion coefficients. Once F and G are determined, we have an analytic expression, Eq. (4), for the scalar potential of a magnetic field that satisfies Maxwell's equations.

We expand the functions F and G in a series of known functions (f, g) and write

$$F_m(z) = \sum_j a_{m_j}f_j(m;z), \quad G_m(z) = \sum_j b_{m_j}g_j(m;z); \quad (17)$$

these functions might depend on the harmonic number m. Functions f and g are chosen to ensure rapid series convergence in Eqs. (17) and to minimize the number of z derivative terms required in Eqs. (13) to (16). Combining Eqs. (13) to (17) and fitting (generally using a least-squares minimization method) the resulting equations to the mapping data, reduced to the form in Eqs. (1) and (2), determine the expansion coefficients a_{m_j} and b_{m_j}.

Example

We use a Fourier sine and cosine series for the expansion functions in Eqs. (17) and assume periodic boundary conditions. Let L be the total length of a magnet plus its significant fringe field region. Equations (17) become

$$F_m(z) = a_{m_0} + \sum_{j=1}^{\infty}\left[a_{m_j}\cos(2\pi jz/L) + b_{m_j}\sin(2\pi jz/L)\right] , \quad (18)$$

$$G_m(z) = c_0 + \sum_{j=1}^{\infty}\left[c_{m_j}\cos(2\pi jz/L) + d_{m_j}\sin(2\pi jz/L)\right] , \quad (19)$$

where $-L \leq z \leq L$. Substituting Eqs. (18) and (19) into Eqs. (13) to (16) and keeping only the first order term in δz_C gives

$$A_{r_m}^a(z_C) \simeq a_{m_0} K_r(m,0) + \sum_{n=0}^{\infty} K_r(m,n) \delta z_C \sum_{j=1}(-1)^n \left(\frac{2\pi j r_C}{L}\right)^{2n}$$

$$\times \left[a_{m_j}\cos(2\pi j z_C/L) + b_{m_j}\sin(2\pi j z_C/L)\right] \quad , \qquad (20)$$

etc. Because of the $(2\pi j r_C/L)^{2n}$ coefficients in Eq. (20), the higher-frequency Fourier components require more terms in the series (sum on n) in Eq. (20) than the lower frequency components.

Equations (1), (2), (20), etc., determine the expansion coefficients (a_{m_j}, b_{m_j}, c_{m_j}, d_{m_j}). One method for obtaining the expansion coefficients is to use a least-squares minimization technique. Define

$$I_m = \sum_{i=1}^{M}\left[A_{r_m}(z_C = z_i) - A_{r_m}^a(z_C = z_i)\right]^2 \quad , \qquad (21)$$

etc., where M denotes the number of measurement values. The function I_m is minimized with respect to the coefficients (a_{m_j}, b_{m_j}, c_{m_j}, d_{m_j}). The resulting set of linear equations is solved for the coefficients. Given the expansion coefficients, the magnetic scalar potential is calculated from Eqs. (3), (4), (18), and (19).

Measurement Coil Positioning

Consider the effect on a magnetic field map where the mapping cylinder center is offset in a single-harmonic multipole magnet. We ignore the fringe-field region and determine the offset map where the magnetic field is constant in z. Equation (4) in a uniform-field region with a single multipole can be written as

$$V_m = V_0 \left(\frac{r}{r_a}\right)^m \cos(m\theta + \theta_m) \quad , \qquad (22)$$

where V_0 and θ_m are constants. Assume that the center of the mapping cylinder is displaced by the distance r_0 and angle θ_0 from the magnet center. Then,

$$\vec{r} = \vec{r}_0 + \vec{r}_C \quad , \qquad (23)$$

where the subscript C denotes the mapping cylinder coordinates. Sine and cosine functions are written as exponentials and the potential function is expanded using the binomial theorem to obtain the potential function in the offset coordinate system. From Eq. (22) we obtain

$$\frac{V_m}{V_0} = \left(\frac{r}{r_a}\right)^m \cos(m\theta + \theta_m)$$

$$= \frac{1}{r_a^m}\sum_{n=0}^{m}\frac{m! r_0^n r_C^{m-n}}{n!(m-n)!}\cos[n\theta_0 + (m-n)\theta_C + \theta_m] \qquad (24)$$

$$= \frac{1}{r_a^m}[r_C^m \cos(m\theta_C + \theta_m) + ...$$

$$+ r_C(mr_0^{m-1})\cos\{\theta_C + [(m-1)\theta_0 + \theta_m]\} + const.] . \quad (25)$$

Equation (24) is the general form of the magnetic scalar potential for a displaced mapper centroid. Equation (25) lists only the dipole and m^{th} harmonic terms. The mapper measurement gives

$$V = A_m \cos(m\theta_C + \theta_m) + ... + A_1\cos(\theta_C + \theta_1) \quad , \qquad (26)$$

where A_m and A_1 are the m-harmonic and dipole amplitudes, respectively. Equation (25) shows that the ratio of the dipole to the $2m$-pole harmonic strengths is mr_0^{m-1}/r_C^{m-1}, from which we can calculate r_0. The dipole phase angle $\theta_1 = (m-1)\theta_0 + \theta_m$ and, therefore,

$$r_0 = \left(\frac{A_1}{mA_m}\right)^{1/(m-1)} r_C , \qquad (27)$$

$$\theta_0 = \frac{\theta_1 - \theta_m}{m-1} . \qquad (28)$$

The above analysis is accurate when there is a single dominant multipole in a magnet. The effective center (zero dipole moment) of a compound magnet, containing several different multipole windings (quadrupole + octupole, etc.), will generally move as the relative multipole excitations change because of centroid misalignments. Therefore, the separate multipole components in a compound magnet should be mapped individually.

The analysis indicates that the magnet mapping cylinder does not have to be precision aligned with the magnet center axis. The effect of a mapper center-line offset and constant tilt can be unfolded from the map data.

Further error analysis can be considered once the f and g expansion functions are chosen, the measurement tolerances are determined, and the method for fitting the expansion functions to the data is decided. Beam dynamics requirements will determine the needed accuracy of the magnetic fields and the error analysis effort.

Summary

We have analyzed a magnet mapping scheme, suggested by Halbach[3], using a rotatable constant radius cylinder that is centered and moves on the magnet axis. The magnet map is Fourier analyzed and presented in Eqs. (1) and (2). Equations (13) to (16) are fitted to the map data to determine the functions F and G [in the form of Eqs. (17)], which, when combined with Eq. (4), give the magnetic scalar potential. Equation (3) then gives the magnetic field.

An error analysis was included to determine the effect of an offset mapper center line from the magnet axis in the nonfringe-field region of a magnet. A straightforward (though perhaps tedious) extension of the error analysis can be made in the fringe-field region.

References

1. E. A. Wadlinger, "Fringe Fields of Current-Dominated Multipole Magnets," these proceedings.

2. K. Halbach, "Physical and Optical Properties of Rare Earth Cobalt Magnets," Nuclear Instrum. and Methods **187** (1981) 109-117.

3. K. Halbach, Lawrence Berkeley Laboratory, private communication.